JOURNAL OF MATERIALS SCIENCE 26 (1991) 1955–1970

Matrix effects on lifetime statistics for carbon fibre–epoxy microcomposites in creep rupture

H. OTANI*, S. L. PHOENIX, P. PETRINA
Department of Theoretical and Applied Mechanics, Thurston Hall, Cornell University, Ithaca, New York 14853, USA

Experimental results are presented for the strength and lifetime in creep rupture of carbon–epoxy microcomposites consisting of seven carbon fibres (Hercules IM6) within an epoxy matrix (Dow DER 332 epoxy with Texaco Jeffamine T403 curing agent) in an approximately hexagonal configuration. Special attention was paid to clamping, specimen alignment, shock isolation and accurate lifetime measurement. The results were analysed using a previously developed model, which involves a Weibull distribution for fibre strength and micromechanical stress redistribution around fibre breaks where the matrix creeps in shear following a power law. The model yields Weibull distributions for both microcomposite strength and lifetime where the respective shape and scale parameters depend on model parameters such as the Weibull shape parameter for fibre strength, the exponent for matrix creep, and the effective load transfer length and critical cluster size for failed fibres. Experimental results were consistent with the theory, though a fractographic study suggested time-dependent debonding along the fibre–matrix interface as being a key mechanism. Arguments were given to suggest, however, that the overall analytical forms would essentially be preserved. The results were compared with earlier results using a different epoxy system (Dow DER 331 epoxy with DEH 26 curing agent). Values for the matrix creep exponent and the effective load transfer length were about double and triple respectively the values from the earlier study, leading to slightly reduced strength, about one-half the variability in lifetime, but almost one-half the value of the exponent for the power law relating microcomposite lifetime to stress level.

1. Introduction

For almost three decades, research has been conducted to develop lightweight, filamentary composite structures which can reliably sustain high tensile loads for long times. An important material for such applications is carbon fibres in a polymer matrix such as epoxy, and possible structures include filament-wound pressure vessels, flywheels, gas centrifuges, rocket motor casings, structural beams, and tension members in cables for cable-stayed bridges. In many such settings, failures can have disastrous consequences.

In the above applications the composite is subject to creep rupture (variously called stress rupture, creep fatigue, static fatigue and stress-life rupture), a highly random and catastrophic phenomenon. Experimental studies on resin impregnated strands (see Phoenix *et al.* [1] for a review of the literature) show large statistical variations in lifetime for ostensibly identical specimens. More importantly, the sensitivity of median lifetime to stress level, as represented say by a power law, varies widely with the composite material system and may show substantial variation in the power exponent even for systems with apparently similar fibre and matrix mechanical properties. Moreover, the shapes of the lifetime distributions, especially in the lower tails important to reliability calculations, may differ unexpectedly. This variation introduces large uncertainty in establishing structural reliability.

Failure in these composites is generally a complex statistical process involving scattered failure of fibres at flaw sites, overloading of neighbouring fibres by way of stress transfer through the matrix, and the growth of clusters of adjacent fibre breaks to a critical, unstable size. In creep rupture, failure is generally driven by a combination of thermally activated flaw growth and failure in the fibres, viscoelastic creep in the matrix near fibre breaks, and progressive debonding at the fibre–matrix interface. The latter two mechanisms result in a widening pattern of overloading on fibres next to existing breaks causing additional breaks. The result is a sequence of adjacent fibre breaks which grow in time and form small clusters, one of which becomes catastrophically unstable.

In carbon fibre–polymer matrix composites it is often assumed that the graphite fibres themselves are virtually immune (at room temperature) to creep rupture, so that matrix creep and progressive interface debonding are the key time-dependent mechanisms. Far-

* *Present address*: Nissan Motor Company, Ltd., Aerospace Division, 3-5-1, Momoi, Suginami-ku, Tokyo, Japan

0022–2461/91 $03.00 + .12

quhar *et al.* [2] recently studied the creep rupture of single Hercules IM6 graphite fibres, and while measurable creep rupture was observed, the power-law exponent relating median lifetime to stress level was about 300. This value is several times larger than the value for the exponent determined by Phoenix *et al.* [1] for microcomposites of the same fibres in an epoxy matrix, and will be almost an order of magnitude larger than the values reported here. Thus, we will be justified in neglecting the creep rupture of the fibres in modelling and interpretation of our experimental results.

The main purpose of the present paper is to report and interpret strength and creep-rupture results on carbon–epoxy microcomposites consisting of seven carbon fibers (Hercules IM6) within an epoxy matrix (Dow DER332 epoxy with Texaco Jeffamine T403 curing agent) in an approximately hexagonal configuration and tested at a 30 mm gauge length. Special attention has been paid to clamping, specimen alignment, shock isolation and accurate lifetime measurement; thus the main shortcomings of the earlier study [1] in our laboratory on a similar system (Hercules IM6 fibres in Dow DER 331 epoxy with DEH 26 curing agent), have been largely overcome, especially with respect to shock and vibration isolation. The experimental methodology is similar to that in the earlier study, so we discuss only key departures in the techniques. The results will be analysed using the theoretical model developed there, and beyond restating some key results, we refer the reader to that work for details of the derivation and full interpretation. Since major differences emerge in the behaviour of the respective epoxies for the two studies, we will also mention briefly some experiments performed using the single-fibre-composite test as described in Netravali *et al.* [3].

2. Review of theoretical concepts and key results

2.1. Statistical model for strength of single fibres

The strength of a single fibre, randomly sampled from a yarn and uniformly loaded over a gauge length l_0, is assumed to follow a Weibull distribution of the form

$$F(\sigma) = 1 - \exp[-(\sigma/\sigma_{l_0})^{\zeta}] \quad \sigma \geqslant 0 \qquad (1)$$

where ζ and σ_{l_0} are the Weibull shape and scale parameters respectively. Following Watson and Smith [4], and Gutans and Tamuzs [5] the scaling of strength with gauge length is embodied in the Weibull scale parameter through the relationship

$$\sigma_l = \sigma_{l_0}(l/l_0)^{-\alpha/\zeta} \qquad (2)$$

where the parameter α typically lies between 0 and 1. The value $\alpha = 1$ corresponds to the usual, weakest-link scaling of Poisson process assumptions on the random occurrence of flaws along the fibre. A value $\alpha < 1$ is said to reflect random variations in such things as diameter and material texture of fibre specimens sampled from *across* a yarn, variations which are not revealed when sampling specimens from *along* a continuous filament.

In the model for composite strength, we will have interest in the strength of fibre elements of a characteristic length δ, called the effective load transfer length. Accordingly we denote $F_\delta(\sigma)$ as the Weibull distribution function (Equation 1) for the strength of such a fibre element having shape parameter ζ and the scale parameter

$$\sigma_\delta = \sigma_{l_0}(\delta/l_0)^{-\alpha/\zeta} \qquad (3)$$

Typically δ is more than two orders of magnitude shorter than the typical gauge length of tension tests, so that estimation of σ_δ by experiment or extrapolation must be carried out with due care (see Henstenburg and Phoenix [6] and Gulino and Phoenix [7] for recent theoretical and experimental developments).

2.2. Statistical model for microcomposite strength

The model for the strength of the microcomposite of length, l, is often referred to as the chain-of-bundles model as shown in Fig. 1. The composite is viewed as being partitioned into a chain of m bundles where $m = l/\delta$, and each bundle has n fibre elements of length δ where $n = 7$ in the present case. Within each bundle, the load of broken fibres is shifted to nearby neighbours according to a local load redistribution rule given in terms of load concentration factors $K_1 < K_2 < \cdots < K_k < \cdots$, where the value of the subscript generally refers to the number of adjacent broken fibres. (For simplicity in the exposition, we ignore certain subtleties in the definitions of δ and the K_i, as described in Phoenix *et al.* [1], but will refer to these where relevant in the discussion of the experimental results.)

We let $H_{m,n}(\sigma)$ be the distribution function for the strength of the microcomposite, and following Phoenix *et al.* [1] let

$$d'_1 = 1 \qquad (4)$$

$$d'_2 = (1/7)[6(7/6)^{\zeta} + 18(4/3)^{\zeta}] \qquad (5)$$

and

$$d'_3 = (1/7)[36(4/3)^{\zeta}(5/3)^{\zeta} + 12(7/6)^{\zeta}(17/10)^{\zeta} + 36(7/6)^{\zeta}(6/5)^{\zeta} + 12(4/3)^{\zeta}(17/10)^{\zeta}] \qquad (6)$$

where, in principle, $d'_4, \ldots, d'_7$ may be calculated but are not needed for the present analysis. The key result

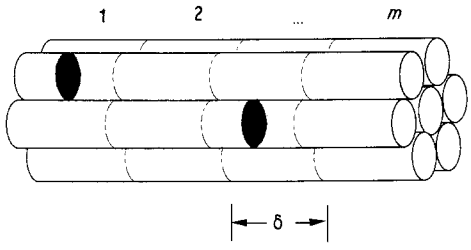

Figure 1 Idealized model of the seven-fibre composite (matrix not shown). δ fibre element length, m number of bundles, • single fibre break).

is

$$H_{m,7}(\sigma) \approx 1 - \exp[-m7d'_k(\sigma/\sigma_\delta)^{k\zeta}] \quad \text{for} \quad \sigma_k < \sigma < \sigma_{k-1} \tag{7}$$

and $k = 1, 2, 3, \ldots, 7$, where $1 > \sigma_1 > \sigma_2 > \sigma_3 \ldots$ are stress transition points as described shortly. These k values are referred to as "critical values" as they represent the size of a cluster of breaks at the onset of instability and fracture for that particular stress. We may rewrite Equation 7 as

$$H_{m,7}(\sigma) \approx 1 - \exp[-(\sigma/\sigma_{k,m,7})^{k\zeta}] \tag{8}$$

where

$$\sigma_{k,m,7} = \sigma_\delta(m7d'_k)^{-1/(k\zeta)} \tag{9}$$

The stress transition points, σ_k, were initially defined most naturally as σ_δ/κ_k where $\kappa_0 = 1$, $\kappa_1 = 4/3$, $\kappa_2 = 17/10, \ldots, \kappa_6 = 7$ and $\kappa_7 = \infty$, these having been derived from the K_k for the dominant failure configurations. These points, however, produce small discontinuities in the approximation to $H_{m,7}(\sigma)$ at the stress boundary points $\sigma_\delta/\kappa_1, \sigma_\delta/\kappa_2, \ldots$. An approximation to $H_{m,7}(\sigma)$, which has a smoother appearance graphically, is constructed from the inner envelope formed by the Weibull distributions of Equation 7, where the stress transition points are then determined from the intersection points of these distributions and are given by

$$\sigma_k = \sigma_\delta(d'_k/d'_{k+1})^{1/\zeta} \quad k = 1, 2, 3, \ldots \tag{10}$$

We use these points in the subsequent analysis.

In tension testing microcomposite specimens of a given volume $V = 7m$, one of the above Weibull distributions will tend to dominate, being the one which defines the median and about which much of the data will empirically fit. In past work [8, 9] the k value for this Weibull distribution has been referred to as the (dominant) critical cluster size k^*. We let $\zeta_c = k^*\zeta$ and $\sigma_c = \sigma_{k^*,m,7}$, and write

$$H_{m,7}(\sigma) \approx 1 - \exp[-(\sigma/\sigma_c)^{\zeta_c}] \tag{11}$$

as the dominant Weibull approximation for the strength of the microcomposite. In the case of the microcomposites tested in this paper we will find $k^* = 2$. Thus, insofar as a single Weibull distribution is acceptable for representing the strength of a microcomposite, ζ_c and σ_c are the respective Weibull shape and scale parameters.

2.3. Statistical model for microcomposite lifetime in creep rupture

The key feature in the creep rupture of a microcomposite is the time-dependent growth of the effective load transfer length, δ, which is caused by viscoelastic creep of the matrix under shear, or progressive debonding in time (discussed in a later section). As in the case of short-term strength, the failure process is initiated by individual fibre breaks, which cause overloads in neighbouring fibres through the matrix along the length δ. Some of these neighbouring fibres may fail instantly because of the overloads, but others may fail later due to an increase in δ with time, thus, the number of fibre breaks increases as time goes by, and if one of the clusters of fibre breaks reaches a critical size, k', catastrophic failure of the microcomposite results.

In the case of matrix creep, the matrix is modelled as a linearly viscoelastic medium having a power-law creep function of the form

$$J_m(t) = J_0[1 + (t/t_0)^\theta], \quad t \geqslant 0 \tag{12}$$

where θ and t_0 are the creep exponent and time constant respectively, and $J_0 = 1/G_m$ where G_m is the elastic shear modulus of the matrix. From Lagoudas *et al.* [10] one may argue that the effective load transfer length associated with a cluster of fibre breaks grows approximately as

$$\delta(t) \approx \delta[1 + (t/t'_0)^\theta]^{1/2}, \quad t \geqslant 0 \tag{13}$$

where δ is the effective load transfer length at time zero (elastic solution), and t'_0 is a time constant, which is close to t_0 in value.

For an overstressed fibre element next to i contiguous breaks that have occurred at time zero, we let $F_\delta(t; \sigma_i)$ be its distribution function for lifetime, where $\sigma_i = K_i\sigma$. Then at longer times, as $\delta(t)$ grows much larger than δ, Phoenix *et al.* [1] argue that approximately

$$F_\delta(t; \sigma_i) = 1 - \exp[-(K_i\sigma/\sigma_\delta)^\zeta(t/t'_0)^{\alpha\theta/2}] \approx (K_i\sigma/\sigma_\delta)^\zeta(t/t'_0)^{\alpha\theta/2}], \quad t \gg t'_0 \tag{14}$$

where the last approximation holds only when its value is less than one. This intermediate result embodies the increased hazard to an overloaded fibre element as δ increases in time following Equation 13, and illustrates how the various parameters are ultimately connected.

We let $H_{m,7}(t; \sigma)$ be the distribution function for lifetime of a microcomposite at stress level σ. The shape of the lifetime distribution depends on the level σ relative to the stress boundary points σ_k of the distribution for strength, as given by Equation 10. We give only the forms relevant to the experimental results discussed later.

First, we consider the highest stress range above σ_1. If $\sigma > \sigma_1$, then the composite fails instantly on loading if any fibre fails, but if no fibre fails the composite lasts indefinitely (under our assumption that the fibres themselves are immune to creep rupture), thus, from Equation 7 with $k = 1$ we have

$$H_{m,7}(t; \sigma) \approx 1 - \exp[-m7(\sigma/\sigma_\delta)^\zeta], \quad t \geqslant 0 \quad \text{and} \quad \sigma_1 < \sigma \tag{15}$$

This is a very high stress level which is not chosen in practice, and the probability of survival on loading is exceedingly small.

Next we consider the stress range $\sigma_2 < \sigma < \sigma_1$. Here we are in the range $k = 2$ for strength and the distribution function for lifetime turns out to have the form

$$H_{m,7}(t; \sigma) \approx 1 - \exp[-m7\phi_2(t; \sigma)] \quad t \geqslant 0 \quad \text{and} \quad \sigma_2 < \sigma < \sigma_1, \tag{16}$$

where

$$\phi_2(t; \sigma) = \begin{cases} d'_2(\sigma/\sigma_\delta)^{2\zeta} & 0 < t < t'_0 \\ d'_2(\sigma/\sigma_\delta)^{2\zeta}(t/t'_0)^{\alpha\theta/2} & t'_0 < t < t_1^\# \\ d'_1(\sigma/\sigma_\delta)^\zeta, & t_1^\# < t \end{cases} \tag{17}$$

and

$$t_j^{\#} = t_0'[(d_{j+1}'/d_j')^{1/\zeta}(\sigma/\sigma_\delta)]^{-2\zeta/(\alpha\theta)} \quad (18)$$

where $j = 2$. Thus the lifetime distribution has three regions. The early region up to the time t_0' is governed by the probability of initial failure (strength distribution) before the matrix has had sufficient time to creep. The second region, $t_0' < t < t_1^{\#}$, corresponds to the creep-driven failure of a fibre element next to an initially broken element (where the time component comes from Equation 14) followed instantly by catastrophic failure. The third region, $t_1^{\#} < t$, is the "eventual failure" region corresponding to the probability that at least one fibre fails initially to start the process; otherwise the microcomposite lasts forever.

Lastly we consider the stress range $\sigma_3 < \sigma < \sigma_2$. This is in the range $k = 3$ for strength and the distribution function for lifetime turns out to have the form

$$H_{m,7}(t;\sigma) \approx 1 - \exp[-m7\phi_3(t;\sigma)], \quad t \geqslant 0 \quad \text{and} \quad \sigma_3 < \sigma < \sigma_2 \quad (19)$$

where

$$\phi_3(t;\sigma) = \begin{cases} d_3'(\sigma/\sigma_\delta)^{3\zeta} & 0 < t < t_{0,2}^* \\ d_3'(\sigma/\sigma_\delta)^{3\zeta}(t/t_{0,2}^*)^{\alpha\theta}, & t_{0,2}^* < t < t_2^{\#} \\ d_2'(\sigma/\sigma_\delta)^{2\zeta}(t/t_0')^{\alpha\theta/2}, & t_2^{\#} < t < t_1^{\#} \\ (\sigma/\sigma_\delta)^{\zeta}, & t_1^{\#} < t \end{cases} \quad (20)$$

and

$$t_{0,2}^* = t_0'[\Gamma(1+\alpha\theta)/\Gamma(1+\alpha\theta/2)^2]^{1/(\alpha\theta)}, \quad (21)$$

and where $t_2^{\#}$ is given by Equation 18, typically $t_{0,2}^* \approx t_0'$. Thus the lifetime distribution has four regions. The early region up to the time $t_{0,2}^*$ is governed by the probability of initial failure (from the strength distribution) before the matrix has had sufficient time to creep. The second region, $t_{0,2}^* < t < t_1^{\#}$, corresponds to the creep-driven failure of a fibre element next to an initially broken element, followed by creep-driven failure of a second fibre element, and followed by catastrophic failure. The third region $t_2^{\#} < t < t_1^{\#}$, corresponds to the creep-driven failure of a fibre element next to an initially broken element followed by catastrophic failure. The fourth region, $t_1^{\#} < t$, is the "eventual failure" region corresponding to the probability that at least on fibre fails initially; otherwise the microcomposite lasts forever.

In the lifetime experiments on microcomposite specimens of a given volume $V = 7m$ and loaded at a given stress level σ, the lifetime distribution will tend to be an approximate Weibull distribution over much of the time range. In the highest practical stress range $\sigma_2 < \sigma < \sigma_1$ this Weibull distribution is determined by middle component of Equation 17, and is given by

$$H_{m,7}(t;\sigma) \approx 1 - \exp[-(t/t_c(\sigma))^{\beta}], \quad t \geqslant 0 \quad (22)$$

where

$$t_c(\sigma) = t_0'(\sigma/\sigma_{2,m,7})^{-\rho^*} \quad (23)$$

$$\beta = \alpha\theta/2 \quad (24)$$

$$\rho^* = 2\rho \quad (25)$$

and

$$\rho = 2\zeta/(\alpha\theta) \quad (26)$$

Actually this distribution will dominate for σ near the lower part of its range where the probability of failure on loading is least.

In the upper part of the next lower stress range, $\sigma_3 < \sigma < \sigma_2$, the above Weibull distribution (Equations 22 to 26) will continue to dominate at longer times, but a second Weibull distribution will begin to emerge in the lower tail. This Weibull distribution is determined by the second component of Equation 20, and is given by Equation 22 where

$$t_c(\sigma) = t_{0,2}^*(\sigma/\sigma_{3,m,7})^{-\rho^*} \quad (27)$$

$$\beta = \alpha\theta \quad (28)$$

and

$$\rho^* = 3\rho/2 \quad (29)$$

This distribution will increasingly dominate as σ takes values near the lower part of this stress range.

As the stress range is lowered still further (which would be practically necessary for larger composites) an approximate Weibull distribution would still dominate, though β would continue to increase as $\alpha\theta k'/2$ and ρ^* would decrease towards the limit ρ, as the critical cluster size k' increases. Note that ρ^* represents the exponent of the power-law relationship between lifetime and stress level, being proportional to ζ, the Weibull shape parameter for fibre strength and inversely proportional to the creep exponent θ for the matrix and the factor α for the length effect in fibre strength. A smaller value of α clearly reduces the susceptibility of overloaded fibres to failure due to matrix creep.

3. Experimental procedure

3.1. Materials used

The fibres used for this experiment were IM6 carbon fibres supplied by Hercules Inc., a high-performance, intermediate modulus, polyacrilonitrile-based fibre suggested for use in prepregging and filament winding. The fibres are approximately 5 μm in diameter. The fibre had been surface treated to improve its interlaminar shear strength, and was supplied as a 12 000 filament tow with sizing.

The epoxy resin used was Dow DER 332 mixed with Texaco Jeffamine T403 curing agent. This epoxy assured uniform performance, had a relatively low viscosity (4 to 6 Pa sec) and had a clear colour because of its high purity and lack of polymer fractions. Its epoxide equivalent weight ranged from 172 to 176 and its chemical reactivity was low. The T403 curing agent, which is a primary triamine with six reactive hydrogens, gives a long potting life to the resin (advantageous for filament winding) thus facilitating the dipping process. The epoxy and curing agent were mixed in proportions of 44 parts to 100 parts by weight of curing agent and epoxy respectively.

3.2. Procedure for extracting and tension testing of single fibres

Single fibres were extracted from the IM6 tow to prepare specimens for tension tests at gauge lengths of

10, 30 and 100 mm in sample sizes of about 50. To extract these filaments, a section of tow measuring 300 mm was cut from the IM6 spool and submerged in a jar of dichloromethane for 1 h to remove the sizing. This sizing had held the fibres in a tightly packed bundle of 12 000, and made it impossible to extract fibres without breaking them. The tow was subsequently placed in a tray filled with distilled water and individual filaments were carefully pulled from the water and placed on a platform covered with Teflon coated paper.

To determine the linear density (mass per unit length), and thus, the cross-sectional area of each 300 mm filament, we removed about 60 mm from one end and placed it in an electrostatically driven vibroscope built in our laboratory [11]. The cross-sectional area was calculated assuming a mass density of 1.73 g cm^{-3}.

For tension testing the single fibre specimens, the tabbing method developed by Wagner *et al.* [12] was used to hold each fibre. The adhesive used was 910 Fs-Gold adhesive, which is a quick-setting methyl cyanoacrylate produced by the Permabond Corporation. From each remaining 240 mm filament section, specimens with gauge lengths of 10, 30 and 100 mm, respectively, were constructed in succession along the fibre, leaving spaces sufficient for tabbing and paying special attention to alignment. Tension tests were performed on an Instron model 1130 machine at a strain rate of 0.025 mm^{-1} and paying special attention to alignment. Conditions were standard ambient conditions of 21 °C and 65% relative humidity.

3.3. Procedure for fabricating seven-fibre microcomposites

For the microcomposites single filaments were first extracted from a 400 mm section of IM6 tow and were measured for their cross-sectional area using the same methods as described above for the tension tests. To achieve uniformity in cross-sectional area, however, only those filaments with a cross-sectional area within 5% of the mean were used to construct the microcomposites, and the rest were discarded.

To make the microcomposites, seven filaments were carefully gathered into a bundle. The most important and difficult aspect of this process was to draw the seven fibres into a bundle without the fibres twisting together at any point, thus precluding a hexagonally-shaped microcomposite. By careful alignment of the fibres and drawing the bundle through a tray of distilled water, the surface tension brought the fibres together uniformly into a bundle.

These seven-fibre bundles were mounted on dipping frames, one of which is illustrated in Fig. 2. The frames and dipping system were the same as those used by Phoenix *et al.* [1], and each frame had the capacity to mount six bundles at a time and hold them during the dipping process into the epoxy system. One end was glued to the top of the frame by extra fast-setting epoxy while a light weight (about 0.2 g) was hung at the other end. After the glue at the top of the frame hardened, the other end was also glued under tension using the light weight (see Fig. 2).

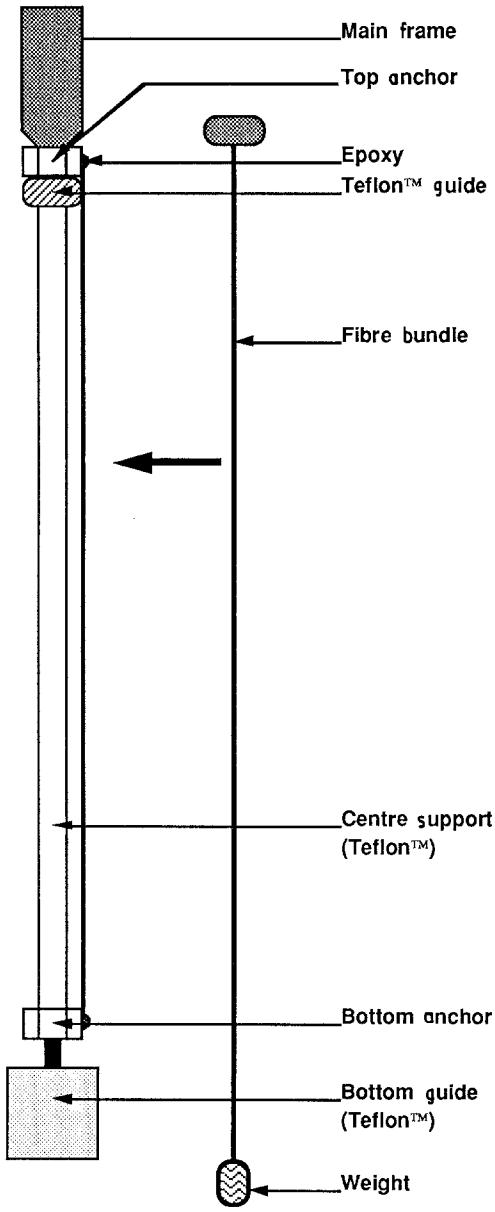

Figure 2 Dipping frame for seven-fibre bundles.

To clean the fibres, the dipping frames holding the bundles were immersed in a cylindrical bath filled with acetone for 5 min to remove oil and other contaminants. After preparing the epoxy, a Pyrex bath cylinder was warmed up to 50 °C just before pouring epoxy into it so that the temperature of the epoxy would not decrease during the dipping process. The frame with bundles was lowered into the epoxy bath at 70 mm min^{-1} and lifted out at 35 mm min^{-1}, using the mechanism shown in Fig. 3 whereby two frames could be dipped in one run. These dipping conditions were determined by trial-and-error to minimize the formation of epoxy beads on the microcomposites. The surface tension of the epoxy tended to pull the fibres into a tight bundle with an approximately hexagonal configuration. By this process it was possible to produce 48 microcomposite specimens from each run (four per bundle) each with a gauge length of 30 mm. To have a sufficient number of specimens (including spares) five runs were made.

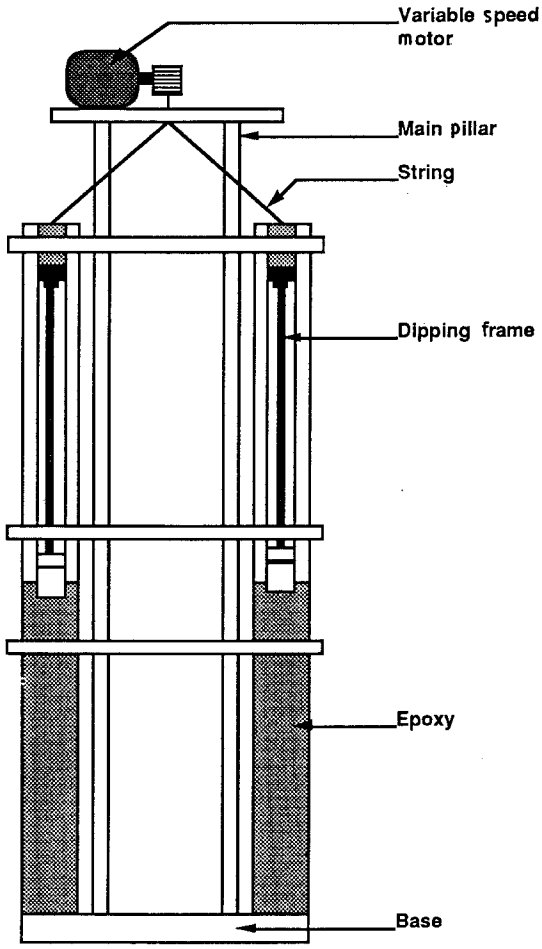

Figure 3 Dipping tower.

After dipping, the frame and long microcomposite specimens were removed from the dipping tower and laid horizontally on a Teflon covered board to cure initially at room temperature for 48 h. Subsequently they were placed in an oven for a second cure cycle at 120 °C for 1 h, and then at 170 °C for 1 h, as recommended for this epoxy–hardener system. Finally, the long specimens were placed on a specially constructed tabbing board, and subdivided into four microcomposite specimens. Each specimen had a 30 mm gauge length and had paper tabs fixed with a fast-setting epoxy adhesive. These microcomposites specimens were randomly allocated as specimens for the tension tests and the creep-rupture tests at three different load levels.

To ensure precise alignment of the microcomposites during testing, threads about 20 mm in length and with end loops were aligned and glued to the ends of each specimen using Duco cement. Loading could then be applied to the loops of the threads. The alignment was confirmed by hanging a light weight on each specimen.

3.4. Procedures for testing of microcomposites

Forty-eight microcomposite specimens were tension tested in order to determine the distribution for short-term strength. The conditions were the same as used for the single fibres (21 °C, 65% RH and strain rate of 0.025 min^{-1}). A Weibull distribution was fitted to the data as will be discussed later in more detail.

The remaining 132 specimens were used in the creep-rupture experiments, with 44 selected at random for each load level. The basic rack was a modified version of the equipment used by Phoenix *et al.* [1]. The applied load levels were 95%, 88% and 83% of the value of the overall Weibull scale parameter for the short term strength, and each load level was tested separately. At each load level, the weights used were identical for all specimens because our fibre screening procedure produced a coefficient of variation of sample cross-sectional area of only about 1.7%, which was much smaller than that of the failure load.

In earlier experiments, Phoenix *et al.* [1] found that external shocks were detrimental to specimen life so that isolation of vibration was essential. In our experiments, a different apparatus from the one used in their experiments was set up with great effort to eliminate external vibration (Fig. 4). This apparatus was actually a modified version of system involving a massive marble table used in the creep-rupture experiments on carbon single fibres by Farquhar *et al.* [2]. In the original apparatus, the platform, on which weights would drop, rested on the same table as the main rack from which specimens were hung. The mass of the weights for the present creep-rupture test were, however more than 70 g, thus, when a specimen broke, a significant vibration would be generated, possibly resulting in another break. Therefore, the platform was placed on the floor while the main rack was mounted on the marble table, which was supported by four low pressure pneumatic springs as shown in Fig. 4. The main rack and marble table weighed approximately 700 kg and the resonant frequency of the system was calculated to be 2 Hz, so the thread length for the specimens was chosen to avoid this resonance condition. The main rack was shielded from dust and air flow in the room by an acrylic cover.

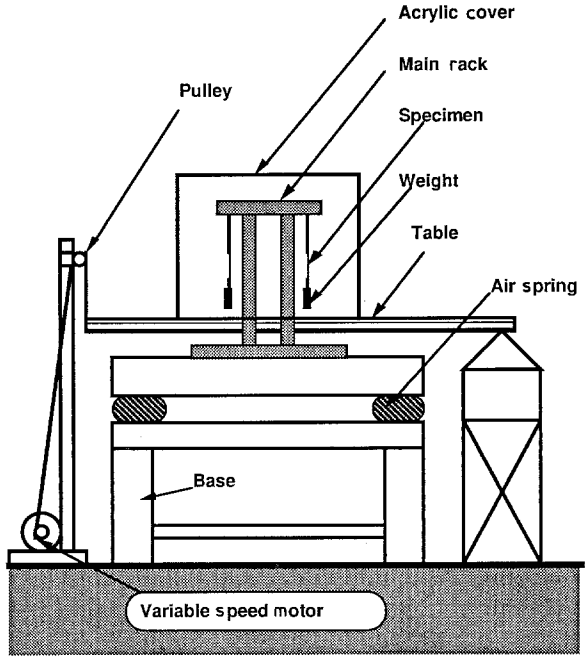

Figure 4 Creep-rupture test apparatus.

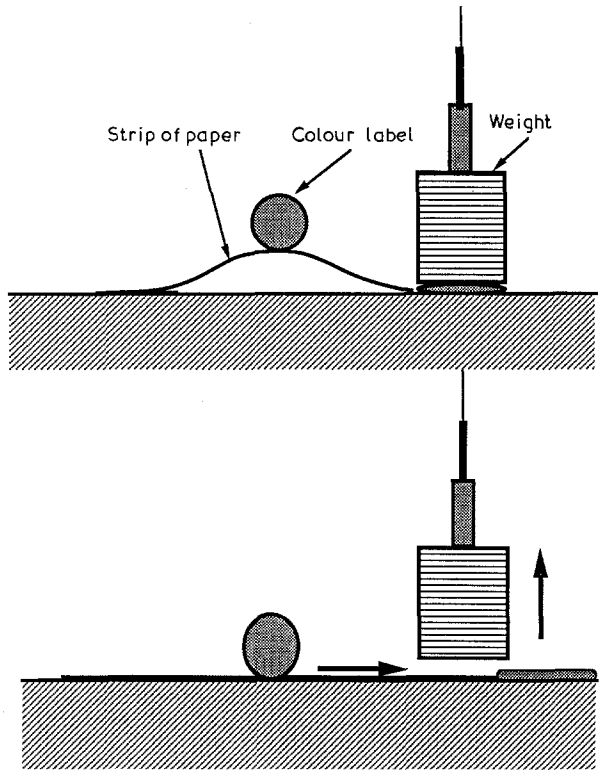

Figure 5 Flag system to indicate starting time.

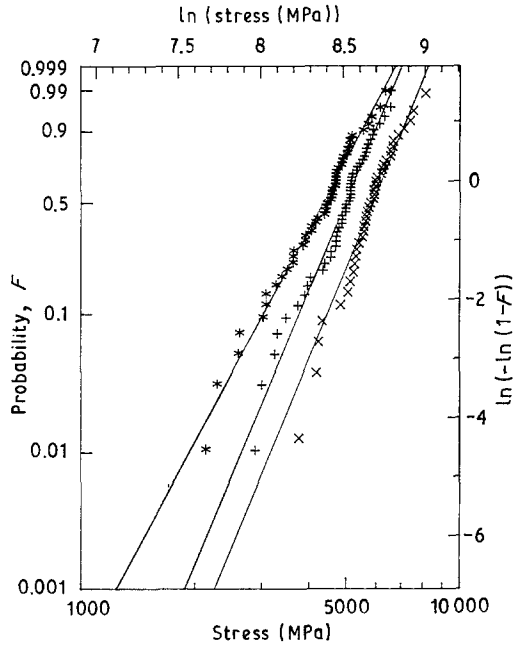

Figure 6 Single fibre strengths on Weibull probability coordinates at gauge lengths (×) 10 mm, (+) 30 mm, and (*) 100 mm.

TABLE I Weibull statistics for tensile strength of single IM-6 fibres

Gauge length (mm)	Number of specimens	Shape parameter	Scale parameter (MPa)
10	39	6.78	6234
30	48	6.73	5277
100	47	5.15	4679

Another modification in the present experiments was a failure time recording system using two video camcorders. Unlike the cantilevered, electrical microswitch system used by Phoenix *et al.* [1], the camcorder system was reliable and completely free of vibration problems. In order to determine exactly when each weight left the platform, thus loading the associated specimen, a thin strip of paper with a coloured "flag" was placed under each weight as shown in Fig. 5. One end was placed directly underneath the weight and the other end was attached to the platform by a self-sticking label so that the thin strip of paper was elastically arched as shown in Fig. 5. This strip of paper flattened when the weight left the platform, so the exact starting time of loading could be determined easily and accurately from the camcorder record.

4. Experimental results and interpretation

4.1. Statistics for fibre strength

Fig. 6 shows plots of the tension test results for the single fibres on Weibull coordinates. Table I presents the maximum likelihood estimates (MLE) of the Weibull shape and scale parameters for failure stress for the three gauge lengths considered. For these specimens, the mean and coefficient of variation of the filament cross-sectional area were respectively 2.53×10^{-5} mm^2 and 8.2%. An interesting feature in the calculations was that the coefficient of variation of filament failure stress was actually slightly larger (by 5 to 20%) than that for failure load at the two shortest gauge lengths, which is opposite to what one might anticipate. This suggests a complex relationship between filament diameter and failure load whereby larger filaments may actually be weaker. Phenomena of this sort were recently studied for a variety of fibres by Wagner [13].

In the fibre strength model of Equations 1 to 3, the correlation factor, α, is assumed to be constant, but the results of the tension tests on single fibres suggest that α may vary slightly with the gauge length. Fig. 7 shows a log–log plot of the Weibull scale parameter for strength against gauge length, including 95% confidence intervals. Such plots are supposed to form a straight line with a slope of $-1/\zeta$ in the standard weakest link model, where $\alpha = 1$. However, Fig. 7 suggests that the slope tends to level off slightly as the gauge length increases, suggesting an increase in ζ. On the other hand, Table I shows that ζ becomes smaller at longer gauge lengths than shorter ones. Taking these features together, it is suggested that α varies slightly with the gauge length and takes slightly smaller values than 1 at the longest gauge lengths. Similar tendencies have been observed for other carbon fibres such as Hercules AS4 and Union Carbide T300 in experiments conducted in our laboratory. Phoenix *et al.* [1] also saw the same trend in IM6 fibres without sizing. Specifically, α for IM6 is close to 1 at less than a 30 mm gauge length (of interest to the models here) but may be about 0.85 at a 100 mm gauge length.

As further verification of the applicability of the weakest-link model, a "master curve", which scales the

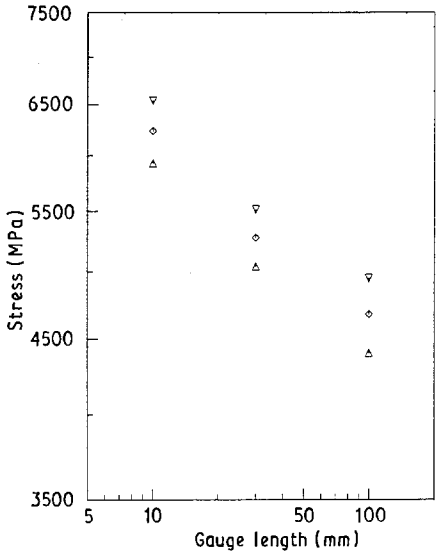

Figure 7 Weibull scale parameter for strength, including 95% confidence interval (∇ upper limit, Δ lower limit) plotted against gauge length on log–log coordinates.

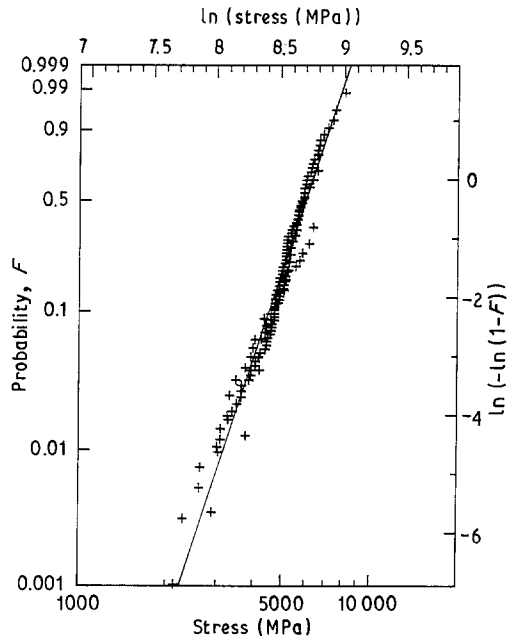

Figure 8 "Master distribution" of all fibre strengths results scaled to a 10 mm gauge length. Weibull parameters are $\zeta = 6.78$ and $\sigma_{10} = 6234$ MPa with $\alpha = 1$.

data for different gauge lengths into one gauge length, was constructed. In the weakest-link setting, the probability of failure, $F_{l_1}(\sigma)$, at a gauge length of l_1, is scaled to another length l_0 as

$$F_{l_0}(\sigma) = 1 - [1 - F_{l_1}(\sigma)]^R \qquad (30)$$

where $R = l_0/l_1$ and $F_{l_0}(\sigma)$ is the scaled probability. Such a scaling is easily obtained on Weibull coordinates since $F_{l_1}(\sigma)$ is shifted vertically by the distance ln(R) on the $\ln[-\ln(1-F)]$ scale. The master curve constructed from the single fibre data at the three gauge lengths scaled to a gauge length of 10 mm, is shown in Fig. 8. This curve is remarkably smooth and straight (apart from the tail variations which are to be expected). A Weibull distribution, with the respective shape and scale parameters of 6.78 and 6234 MPa is also shown. Taking all these aspects into consideration, the Weibull weakest-link model with $\alpha = 1$ is quite appropriate and valid for characterizing the fibre strength at these gauge lengths.

The gauge length, δ, of interest in the model will be less than 10 mm by a factor of about 20. At this length, the Weibull scale parameter for fibre strength, σ_δ, is predicted to be about 9500 MPa using Equation 3. From Fig. 8, we see that this value is only moderately larger than the largest fibre strength observed (8100 MPa), and the shape of the upper tail of the master curve suggests that such an extrapolation is reasonable. Recently Gulino and Phoenix [7] were able to study the strength of IM6 fibres from a different spool at this length scale using special techniques, and observed strengths comparable to those predicted here. However, anomalous fibre to fibre variations across a yarn were also suggested in that study.

Compared to the results of Phoenix *et al.* [1], the values of both the Weibull scale and shape parameters at the gauge lengths tested were considerably larger in our experiments. For example, the scale and shape parameters for a 10 mm gauge length were 5283 MPa and 5.4 respectively in their experiments as compared to 6234 MPa and 6.78 here. Also the largest strength observed in their experiments at a 10 mm gauge length was about 7000 MPa, whereas their value for σ_δ was about 11 500 MPa, which is substantially larger than in our case. Thus the extrapolation of fibre strength required in the microcomposite model was much more severe in their case.

Substantial variations in carbon fibre strength from spool to spool (and even through a spool) are to be expected due to slight variations in processing conditions. Thus, in micromechanical modelling and experimentation as was carried out here, it is necessary to characterize the fibre through extensive tension tests at various gauge lengths.

4.2. Distributions for strength of microcomposites

The strength results for the 45 microcomposite specimens, tension tested at a gauge length of 30 mm, are plotted on Weibull coordinates on Fig. 9. Also shown is a Weibull distribution fitted to the data with MLE values of 13.9 and 4941 MPa for the shape and scale parameters respectively. According to the theoretical arguments given earlier in connection with Equation 11, the microcomposite strength should approximately follow a Weibull distribution, which should dominate over a fairly broad range of load. The effective Weibull shape parameter ζ_c should be $k^*\zeta$ for some integer, k^*, called the critical cluster size. Comparing the value $\zeta_c = 13.9$ above with $\zeta = 6.8$ for the fibre (used henceforth in model calculations) we have $k^* \approx 2$ almost exactly.

While the MLE fit in Fig. 9 is excellent in the upper tail, the slope appears to be steeper in the lower tail. Such an effect was indeed predicted in the discussion associated with Equations 8 to 10. For lower failure stresses, a Weibull distribution with shape parameter

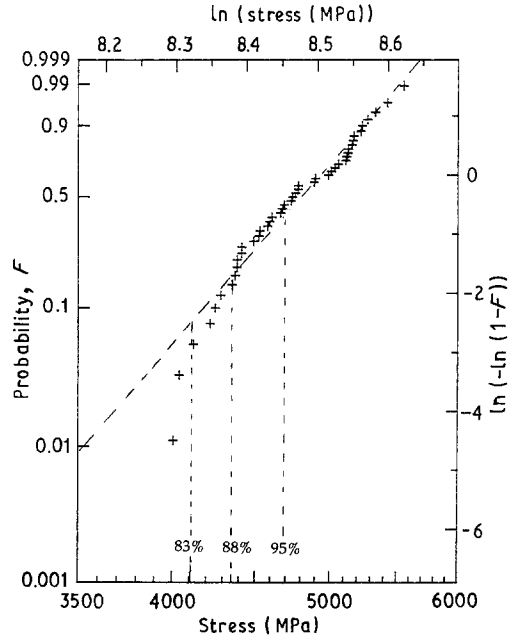

Figure 9 Microcomposite strengths fit to a Weibull distribution at a 30 mm gauge length. MLE parameter estimates are $\zeta_c = 13.9$ and $\sigma_c = 4941$ MPa. Also shown are the three stress levels chosen for the creep-rupture experiments.

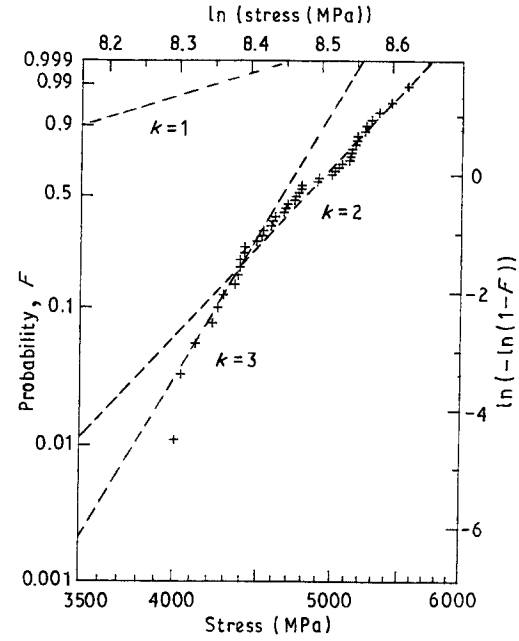

Figure 10 Microcomposite strength on Weibull probability coordinates with tangent Weibull distributions from theory.

3ζ is predicted to fit the actual data. At the same time the extreme upper tail is predicted to follow a Weibull distribution with shape parameter ζ, which in fact is the distribution function for the weakest fibre in the bundle (or all seven fibres connected end to end). Fig. 10 shows a manual fit of these three Weibull distributions to the strength data and the respective scale and shale parameter values are given in Table II along with the MLE values of Fig. 9.

While only 45 specimens were tension tested in the present case, the character of the data and plots on Fig. 10 is strikingly similar to that obtained by

TABLE II Weibull statistics for microcomposite strength

k	Shape parameter	Scale parameter (MPa)
Overall MLE	13.9	4941
1	6.8	3924
2	13.6	4900
3	20.4	4730

Phoenix *et al.* [1] who tested 126 specimens. In both cases, the plots clearly consist of two segments and follow the fitted Weibull distribution very well. These results support our theory that the critical cluster size actually varies with the stress level. Also, the scale parameter values in Table II should then correspond to $\sigma_{1,m,7}$, $\sigma_{2,m,7}$ and $\sigma_{3,m,7}$.

The Weibull scale parameter for the microcomposites at a 30 mm gauge length was 4971 MPa, somewhat smaller than that of the single fibres which was 5277 MPa at this length. In contrast, the corresponding values in Phoenix *et al.* [1] were 5154 MPa as opposed to 5283 MPa but at a smaller gauge length of 10 mm.

Using the above results, the effective load transfer length, δ, and the scale parameter, σ_δ, can now be calculated. From Equations 2, 3 and 9, we may write $\sigma_{k,m,7}$ in terms of σ_l, d'_k, ζ and l, the gauge length 30 mm, as

$$\sigma_{k,m,7} = \sigma_l(7d'_k)^{-1/(k\zeta)}(l/\delta)^{(k-1)/(k\zeta)} \quad (31)$$

whence

$$\delta = l(7d'_k)^{-1/(k-1)}(\sigma_l/\sigma_{k,m,7})^{k\zeta/(k-1)} \quad (32)$$

where an intermediate step is

$$\sigma_\delta = \sigma_l(l/\delta)^{1/\zeta} \quad (33)$$

Table III shows the results of the calculation of d'_k, δ and σ_δ for both $k = 2$ and 3. Clearly δ does not have one value but is slightly larger for $k = 3$ than for $k = 2$. This phenomenon was observed also by Phoenix *et al.* [1] where the ratio of the δ values was about 1.66 there as compared to the present ratio, 1.42, which represents slightly better agreement. They explained the difference in terms of local geometric effects, dynamic overload effects, debonding effects, and oversimplified probability calculations for $k = 3$ that ignore certain less likely failure sequences. These differences in δ also mean that Equation 10 will be less accurate in predicting the stress transition points for the Weibull distributions on Fig. 10.

A most striking feature is the fact that the δ values here are three to four times the values in Phoenix *et al.* [1], where a different epoxy was used. Taking $\delta = 0.57$ and $l = 30$ mm we calculate the number of bundles, m, in the microcomposite to be 52, so the composite volume is $V = 7m = 368$ elements as compared to 467 elements in their study. We will return later to possible explanations for this important difference in δ.

It is interesting to calculate the number of microcomposite test specimens that would be required to experimentally reveal the transition between the $k = 1$ and $k = 2$ Weibull distributions on Fig. 10, and produce data in the $k = 1$ region. From Equation 10 we

TABLE III Parameters for Weibull envelope for microcomposite strength

k	d'_k	Effective load transfer length δ (mm)	Scale parameter for length δ σ_δ (MPa)
1	1	—	—
2	20.2	0.57	9499
3	1753	0.81	9013

calculate the stress transition point as 6075 MPa, corresponding to the survival probability $\exp[-(6075/3924)^{6.78}] = 7 \times 10^{-9}$, thus, about one billion tests would be necessary to obtain a few points falling in the $k = 1$ region!

4.3. Lifetime in creep rupture of microcomposites

The stress levels chosen for the creep-rupture experiments were 95%, 88% and 83% of the MLE Weibull scale parameter value (4941 MPa) for microcomposite strength, as illustrated on Fig. 9. Note that one stress level is in the $k = 2$ region, one is in the $k = 3$ region and one is just below the stress transition point between the two regions.

Plots of the lifetime results, on Weibull probability coordinates, are shown in Figs. 11, 12 and 13 for the three stress levels, respectively. The Weibull scale and shape parameter values for the lifetime at each stress level were estimated by the MLE method for censored samples given by Cohen [14]. Tables IV and V present these parameter estimates as well as other important information about the creep-rupture experiments. In particular, we show for the three respective data sets the actual and predicted numbers of initial failures (failures on loading), the numbers of creep-rupture failures, the numbers of censored samples (survivors at the termination of the test) and the test lengths.

With respect to the generation of this data a few comments are in order. During the entire time of loading, the apparatus was able to isolate the specimens completely from vibration, and no failures related to hazardous causes such as door slams, air flow and other external shocks occurred. For example, what appear to be clusters of failure times near 10 000 seconds on Figs 12 and 13, actually are not and represent failures typically several minutes apart.

Although the theoretical model for the Weibull lifetime distribution assumes an ideal step loading, the actual loading history was approximately a ramp loading with a steep gradient. However, the time interval between the beginning of the loading and full loading was calculated to be less than a half a second. The tightness of the paper strip placed underneath each loading weight was adjusted so that it would not move until the applied load to the specimen reached about 99% of the load to be applied. Therefore, the starting time, $t = 0$, could be defined as the moment when the paper strip moved.

The starting time of loading of each specimen was

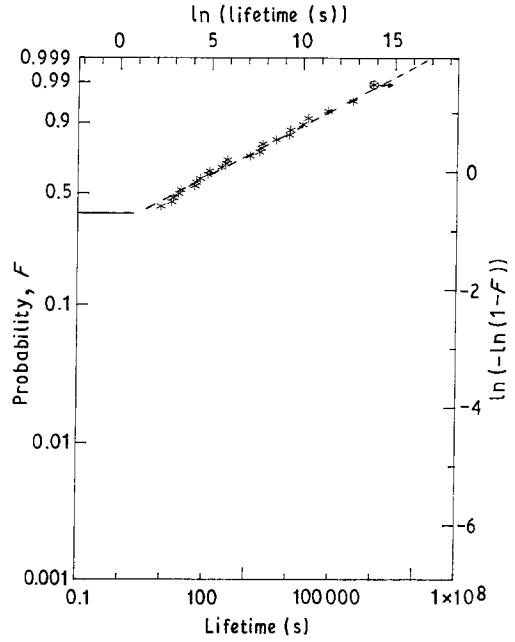

Figure 11 Microcomposite lifetimes at the 95% stress level on Weibull probability coordinates. Weibull distribution has MLE parameters (---) $\beta = 0.175$ and $t_c = 127$ sec.

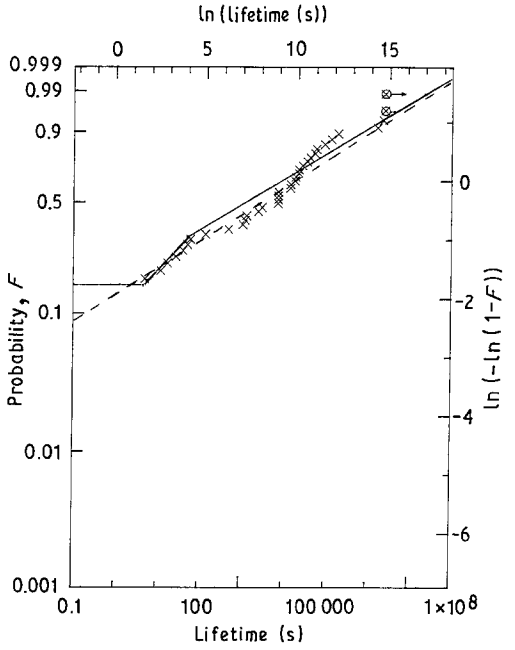

Figure 12 Microcomposite lifetimes at the 88% stress level on Weibull probability coordinates. Manually fitted Weibull distribution to upper tail has parameter values $\beta = 0.18$ and $t_c = 9450$ sec.

measured precisely by the paper strip indicator and a video camcorder, which showed that there was actually a time difference of about 10 seconds between the full-loading time of the first and last specimens due to varying lengths of the alignment threads. Although not all the specimens were loaded simultaneously, the recording system worked so well that we could easily identify the exact starting time for each specimen. This success was very important because interesting behaviour of the microcomposite lifetime was observed in the first 60 seconds as will be discussed shortly. These innovations corrected the major experimental difficulties encountered earlier by Phoenix *et al.* [1].

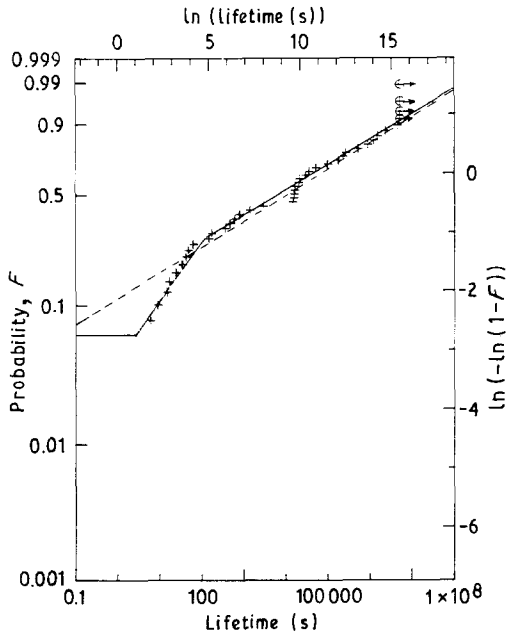

Figure 13 Microcomposite lifetimes at the 83% stress level on Weibull probability coordinates. Manually fitted Weibull distribution to upper tail has parameter values $\beta = 0.18$ and $t_c = 70\,450$ sec.

TABLE IV Overall Weibull statistics for the lifetime of microcomposites

Stress level (%)	Actual stress (MPa)	Sample size	MLE Shape parameter	MLE Scale parameter (sec)
95	4694	43	0.175	127
88	4348	43	0.201 (0.18)*	9475 (9450)*
83	4101	44	0.195 (0.18)*	70 477 (70 450)*

* Estimated from dominant Weibull region of upper tail ($k' = 2$)

TABLE V Various quantities associated with creep-rupture tests

Stress level (%)	Initial failures	Creep-rupture failures	Censored samples	Test length (sec)
95	18 (18)*	24	1	6.0×10^5 (7 days)
88	7 (7)*	34	2	2.5×10^6 (29 days)
83	3 (2)*	37	4	5.0×10^6 (58 days)

* Predicted from envelope fit to tension tests (Fig. 11)

To interpret the creep-rupture data we refer back to the theoretical results given by Equations 16 to 29. For the 95% stress level falling in the $k = 2$ region of microcomposite strength (see Fig. 9). Equations 16 to 18 indicate that there should be *three* time regions of importance with distinct features. For the 88% and 83% stress levels falling in the $k = 3$ region of strength, there should be *four* distinct time regions as indicated by Equations 19 to 21. Actually the experiments were not run sufficiently long to observe the last time region in each case, even at the highest stress level.

As mentioned in Section 2.3, the lifetime distribution is predicted to be a Weibull distribution over much of the time range as given by Equation 22 with parameters given by Equations 23 to 29 depending on the load level. It turns out that for all three load levels here, Equations 23 to 26 apply for the longer times. From the Weibull shape parameter values of Table IV (which are corrected as discussed shortly) we estimate $\beta \approx 0.18$. Earlier we had $\alpha \approx 1$ so that the power-law exponent for matrix creep is estimated $\theta \approx 0.36$.

Turning now to more detailed features of the various distributions, we consider the initial failures and the first time region for each load level. All the initial failures were observed to have occurred just before the time of full loading, that is, the paper slip for a sample did not move as the specimen failed. The earliest creep-rupture failure was at about 5 seconds. Thus initial failures were clearly distinguished from creep-rupture failures.

The numbers of initial failures at each stress level were almost exactly the same as predicted from the short term strength data as shown in Table V. In the experiments, 42% of the specimens (18 out of 43) were initial failures at the 95% stress level, 16% (7 out of 43) at the 88% stress level and 7% (3 out of 44) at the 83% stress level. On the other hand, the predicted percentages of initial failures were 43, 16 and 5%, respectively using the Weibull envelope of Fig. 10.

The upper limit of the first (earliest) time region is t'_0 for the 95% stress level and $t^*_{0,2}$ of Equation 21 for the 88% and 83% stress levels. From the definitions of the first time regions in Equations 17 and 20 respectively, t'_0 and $t^*_{0,2}$ can be estimated as the intersection points between the probability of initial failures and the best fits to the empirical plots for the lower tail regions on Figs. 11 to 13 respectively. Those points were estimated to be about $t'_0 = 3.0$ sec. for the 95% stress level and $t^*_{0,2} = 5.5$ and 2.5 sec. for the 88% and 83% stress levels, respectively. Using the estimates $\theta \approx 0.36$ and $\alpha \approx 1$ in Equation 21 we calculate $t^*_{0,2} \approx 1.14\, t'_0$. Given the rough accuracy of these calculations, the results are fairly consistent. These values are slightly larger than those obtained by Phoenix *et al.* [1].

Next, we consider the second time region for the 88% and 83% stress levels which is $t^*_{0,2} < t < t^{\#}_2$ from the second component of Equation 20. In this region the Weibull distribution Equation 22 actually applies with parameters given by Equations 26 to 29. We estimate respective $t_c(\sigma)$ values of 550 and 2300 sec for the two lower tail regions on Figs 12 and 13 respectively. Theoretically, the upper limit for this time region is $t^{\#}_2$ of Equation 18 which for $\theta \approx 0.36$, $\alpha \approx 1.0$, and $\zeta \approx 6.8$ yields $t^{\#}_2 = 16$ and 118 sec, respectively, for the 88% and 83% stress levels. From the results of the experiments, however, we estimate values of about 45 and 120 sec respectively, though again the resolution is quite rough. Overall the data appear to support the downward bending of the lower tail relative to the rest of the distribution as predicted by the theory. In the micromechanics of the failure process discussed earlier, this behaviour is associated with the 88% and 83% stress levels being in the $k = 3$ region of the strength distribution; such behaviour is not predicted

for the highest 95% stress level and indeed is not observed. In the only vibration-free data set of Phoenix *et al.* [1], which was at the 87.5% stress level, these same features were both predicted and observed.

Next, we consider the third and dominant time region for the 83% and 88% load levels given by the third component of Equation 20; this micromechanical situation also corresponds to the second and dominant time region for the 95% stress level as described by the second component of Equation 17. In all cases the dominant Weibull distribution is Equation 22 with parameters given by Equations 23 to 26. The respective estimates for the Weibull scale and shape parameters for lifetime, $t_c(\sigma)$ and β, as fitted manually, are given in Table IV. These values differ from the previous MLE values because of the removed influence of the lower tail in the present case. (The revised values are used in all calculations henceforth.) Estimates for the various parameters are $\alpha \approx 1.0$, $\beta \approx 0.18$, $\zeta \approx 6.8$, $\theta = 0.36$, $\rho \approx 37$ and $\rho^* \approx 74$. (We consider $\sigma_{2,m,7}$ momentarily.)

To estimate the power-law exponent, ρ^*, there are three approaches. The first approach, which we have applied already, is to determine ρ^* from the basic parameters ζ, θ, and α through Equations 25 and 26; that is $\rho^* = 4\zeta/(\alpha\theta)$. The second approach is to plot, on log–log coordinates, the Weibull scale parameters for lifetime, $t_c(\sigma)$, against stress level for the dominant time regions. According to Equation 23, the slope should be $-\rho^*$. The third approach is to use Equations 23 and 27 directly whereby

$$\rho^* = -\log[t_c(\sigma)/t'_0]/\log[\sigma/\sigma_{2,m,7}] \quad (34)$$

applies for the Weibull dominant time regions and

$$\rho^* = -\log[t_c(\sigma)/t^*_{0,2}]/\log[\sigma/\sigma_{3,m,7}] \quad (35)$$

for the Weibull lower tails with all parameters already calculated including the strength parameters $\sigma_{2,m,7}$ and $\sigma_{3,m,7}$ from Table II.

Fig. 14 shows a plot, on log–log coordinates, of the applied stress, σ, against scale parameter, $t_c(\sigma)$, for the dominant time region ($k' = 2$). From the slope of this plot we estimate $\rho^* = 55$. On the other hand, using Equation 34 we calculate the values 79, 64, and 54 for ρ^* for the stress levels 95%, 88% and 83% respectively.

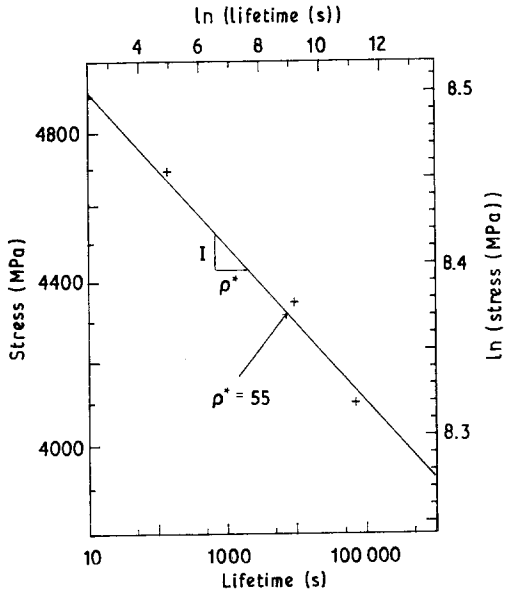

Figure 14 Stress versus Weibull scale parameter for lifetime on log-log coordinates. Fitted power-law has $\rho^* = 55$.

Thus, by the three approaches for estimating ρ^* we have obtained estimates ranging from 79 down to 54. Given the errors inherent in the estimates of the various parameters due to such things as limited sample sizes in both the strength and lifetime, such variation perhaps may be expected. Nevertheless, the cause of these low values appears to stand out, on Fig. 14, as an unexpectedly small value for $t_c(\sigma)$ at the lowest 83% stress level; in fact, $t_c(\sigma)$ appears to increase more slowly with decreasing stress than the model would predict on the basis of the values of the other model parameters.

5. Discussion

5.1. Inconsistencies in values for model parameters

We now pursue possible explanations for the lower than anticipated value of ρ^* from Fig. 14 caused by the value of $t_c(\sigma)$ at the 83% stress level being somewhat less than anticipated. It is easy to see from Fig. 14 for the 83% stress level, that a shift in the value of the scale parameter, $t_c(\sigma)$, to the right by a factor of about *five* would align the points for all stress levels to yield $\rho^* = 64$, whereas a shift by a factor of *ten* would yield a best fit value of $\rho^* = 73$, which would be consistent with our first approach for estimating ρ^* based on Equation 26. Turning to Fig. 13, a deviation in $t_c(\sigma)$ by a factor of five could conceivably be explained on the basis of the natural, random variation in the data, but a deviation by a factor of ten requires another explanation.

It is interesting to consider the increase in the value of $\delta(t)$ for the overloaded fibre that would be necessary for the occurrence of such a reduced value of $t_c(\sigma)$ at the 83% load level. From the scaling factors in Equations 13, 14 and 17 (particularly the dependence $\delta(t) \propto (t'_0)^{-\theta/2}$) one can see that changes in the time scale by the respective factors of five and ten affect $\delta(t)$ at long times by the factors 1.34 and 1.51, respectively. This must be appreciated in terms of the nominal value of the ratio $\delta(t)/\delta \approx 6.3$ at $t = t_c(\sigma) = 70\,477$ sec, assuming $\theta = 0.36$ and $t'_0 = 2.8$ sec. Since $\delta = 0.57$ mm from the results on strength we have $\delta(t) \approx 3.6$ mm at $t = 70\,477$ sec. The above factors of 1.34 and 1.51 increase $\delta(t)$ to 4.8 and 5.4 mm, respectively. Note that corresponding values of the geometric overload factor, δ^*, of Phoenix *et al.* [1] are probably two to three times larger, thus approaching half the specimen length of 30 mm. These values represent large increases in the effective overload length with time far beyond what one might expect to model accurately on the basis of linear viscoelasticity. Increases of this magnitude must involve considerable, time-dependent debonding in addition to matrix creep, evidence for which we discuss shortly. Thus, one

must anticipate that non-linear deformation processes are involved in determining $\delta(t)$.

Phoenix *et al.* [1] mention some implications of a non-linear model for matrix creep as developed by Mason [15]. The matrix material follows a constitutive law with memory, which under a constant shear stress τ_0 has the shear strain

$$\gamma(t) = B\tau_0^{\omega} t^{\theta'} \tag{36}$$

where B, ω and θ' are positive constants. For the overload length $\delta(t)$ we have

$$\delta(t) = Dt^{\theta'/(\omega+1)}\sigma^{(\omega-1)/(\omega+1)} \tag{37}$$

where D is a constant which lumps many model parameters, and we are interested in the implications for long times where $\delta(t) \gg \delta$. Reworking Equations 14 and 17, the exponent on stress in the second component of Equation 17 is now $2\zeta + (\omega - 1)/(\omega + 1)$, and we take $\theta = \theta'/(\omega + 1)$. Thus ρ^* is modified to

$$\rho^{**} = [4\zeta + (\omega - 1)/(\omega + 1)]/\alpha\theta \tag{38}$$

Taking $\alpha = 1$, $\zeta = 6.8$ and $\theta = 0.36$, we find that $\rho^{**} = 64$ and 55 require the *negative* values $\omega = -0.29$ and -0.56, respectively. Unfortunately a negative value for ω is difficult to rationalize on physical grounds since typical non-linearities at high stress levels produce large positive values of ω. Thus, a non-linear law of this form does not appear to explain the results.

The most likely explanation for the above discrepancy is statistical variation in the growth of $\delta(t)$ from specimen to specimen. This variability would result from geometric variation in specimen cross-sectional shape and fibre spacings, or variability connected to the position of the initial fibre break (central or peripheral), or variability in the adhesion of the fibre to the matrix. Such variability would have to be in addition to any initial variations in δ for short term strength in order not to be reflected already in the strength results. (Initial variations in δ must have been minor or they would have decreased the slope of the Weibull line on Fig. 10 for $k = 2$ relative to the respective exponents 2ζ.)

From Equations 25 and 26, $\rho^* = 55$ would require the value $\theta = 0.49$ rather than the value 0.36 which we calculated from Equation 24 using the observed value of $\beta = 0.18$. On the other hand, by Equation 24, $\theta = 0.49$ would correspond to $\beta = 0.24$ rather than the observed 0.18. Thus this variability in $\delta(t)$ would need to depress the value of β by about 25%, which corresponds to an increase in the coefficient of variation of lifetime by about 35%, an effect which we believe is very plausible. Modification of the model to reflect such effects is beyond the scope of the present paper, but a crude calculation is possible to estimate the order of the variability required. As we have already seen, relatively modest changes in $\delta(t)$ have a large effect on lifetimes. The coefficient of variation of lifetime is of the order of 400% for $\beta = 0.24$, and the component introduced by variability in $\delta(t)$ must be slightly less, perhaps 300% (variabilities tend to add following Pythagoras' theorem) to obtain about 550% corresponding to $\beta = 0.18$, as was observed. Since $\delta(t) \propto t^{\theta/2}$, small deviations in $\delta(t)$ are of the magnitude $\theta/2$ times those of t or about 1/4. Thus a coefficient of variation of about 75% in $\delta(t)$ would probably be necessary, a value which is plausible in view of our observations from micrographs of fracture surfaces as we discuss shortly.

5.2. Models for interface debonding as the dominant mechanism for creep rupture

Recently Netravali *et al.* [3] have used the single fibre-composite-test to demonstrate extensive debonding along the interface of a system with Hercules IM6 fibres and Dow 331 epoxy with DEH 26 curing agent, similar to that used in Phoenix *et al.* [1]. Also, using a three-fibre composite system of one IM6 fibre between two larger glass fibres in the same epoxy, Gulino *et al.* [16] have measured the lengths of extensive debonding zones along the fibre with increasing composite stress. Neither study focused on the growth of debonding with time, though the latter study did note stress relaxation in the matrix. To the authors knowledge, models for the time dependent growth of the debond zone through crack growth along the interface have not appeared in the literature. Nevertheless models for Mode I crack growth in viscoelastic materials, as developed by Schapery [17] and by Christensen and colleagues [18, 19], may shed some light especially in the case where the matrix creep compliance assumes a power law as is assumed here. When the creep exponent θ is small, their results indicate that the crack velocity is approximately proportional to $K_I^{2/\theta}$, where K_I is the elastic stress intensity factor. Making the assumption that a similar result would apply to Mode II crack growth in shear, this situation has a similar scaling to the constitutive law described by Equation 36 where $\omega = 2/\theta$ and $\theta' = 1$. Making a further assumption that the reduction in stress intensity factor with increasing $\delta(t)$ has a scaling similar to that which occurred in the analysis leading to Equation 37, one arrives at the approximate result

$$\delta(t) \propto t^{\theta/2}\sigma \quad \text{for } \theta \text{ small} \tag{39}$$

Following the same steps as produced Equation 38, one finds that again $\beta = \alpha\theta/2$ but ρ^* changes to

$$\rho^{**} = 2(2\zeta + 1)/(\alpha\theta) \tag{40}$$

which for typical values of ζ is only slightly larger than ρ^*. In essence, the scaling of the basic results with θ is changed little and in the wrong direction to explain the discrepancy in ρ^* noted above.

The above analysis ignores the potential importance of two other time-dependent aspects of the debonding process. First, chemical adhesion of the epoxy to the fibre is expected to be important, and the kinetics and activation energies of interface decohesion processes may lead to power law exponents different from those for viscoelastic creep, and different also for different epoxies and fibre surface treatments. Furthermore, Whitney and Drzal [20] show significant transverse compressive stresses may exist at the interface due primarily to matrix shrinkage during curing. These compressive stresses lead to frictional

shear stresses behind the debond front which may serve to reduce markedly the Mode II stress intensity factor for crack growth along the interface. Gulino *et al.* [16] experimentally estimated these frictional shear stresses to be of the order of one-half the apparent debond stresses in their three-fibre composites. Should the interface slip in the debond zone following some kintetic process, this would lead to a relaxation of these restraining, frictional shear stresses and an increase the tendency to debond further.

Note that the magnitudes of compressive stresses at the interface depend strongly on the volume fraction of the matrix in the composite. They are probably largest in the single-fibre-composite test and are much lower in the microcomposites of this study because of the closeness of the fibres and the thin layer of epoxy on the surface, as we see shortly. In a typical composite, with a volume fraction of matrix of say 45%, the magnitudes of the compressive stresses would be somewhere in between these two cases.

5.3. Comparison of results with earlier work using a different epoxy

The results obtained here differ in important ways from those obtained earlier by Phoenix *et al.* [1] using similar fibres but a different epoxy matrix (Dow DER 331 epoxy with DEH 26 curing agent). Apart from some minor differences in the strength statistics for the respective fibres, the value of δ was found to be about three times larger and the value of the creep exponent θ nearly double the corresponding values in the earlier work. These differences point to the possibility of important differences in the epoxies and how the epoxies bonded to the fibres. We have found the bulk mechanical properties from standard dogbone specimens of the two epoxies to differ somewhat. The Young's moduli of the two epoxies were approximately equal at about 2000 MPa. The apparent ultimate stresses were, however, respectively 50 MPa here as opposed to 65 MPa there and the epoxy failure strains were about 5 to 6% here as compared with 7 to 9% there. While these differences are in the right direction, they are insufficient in magnitude to explain the large differences in δ and θ.

We also, constructed some single-fibre-composite (SFC) specimens for both epoxies following the procedure of Netravali *et al.* [3]. The mean fragmentation lengths were only about 20% larger for the present epoxy over the previous one, not double to triple as would be required to explain the difference in δ. There were, however, interesting differences in the birefringence patterns at fibre breaks reflecting the tendencies for the epoxies to crack transversely at the fibre break and for debonding at the interface to occur. Both effects appeared to be more prevalent in the present epoxy system. As mentioned, the high volume fraction of epoxy in the SFC test probably results in much higher compressive stresses at the interface than occur in the corresponding seven-fibre microcomposites, so that frictional stresses in the debond zone can be expected to be higher. Also, there are no fibres nearby (as in the three-fibre experiment of Gulino *et al.* [16]) to enhance the shear stresses in the matrix between the fibres. Thus, it is probably unrealistic to expect the SFC test to corroborate the differences observed between the seven-fibre composites of the two studies.

5.4. Studies of microcomposite fracture surfaces

Fig. 15 shows scanning electron micrographs of both a polished cross-section (Fig. 15a) and an outer surface (Fig. 15b) of two microcomposites. About 25% of the specimens had an almost perfectly hexagonal cross-section as in Fig. 1 with the fibres virtually touching, but the remainder had irregularities similar to those shown in Fig. 15a with some fibres almost touching but others with spacings of up to 3 μm. Both the wetting of the epoxy and its bonding to the fibres appeared to be excellent, and before testing the outside surfaces were very smooth as shown except for the occasional benign bead of epoxy. The epoxy thickness of the very outside of the fibres was typically 1/4 to 1 μm, the microcomposites appeared to be void free and the volume fraction of epoxy was about 20%, which is lower than for a typical large-scale composite.

Fig. 16 shows scanning electron micrographs of two fracture zones, one with a single fibre break (a) and one with five broken fibres (b). In the latter case the other two fibres were severed at a point about 30 fibre

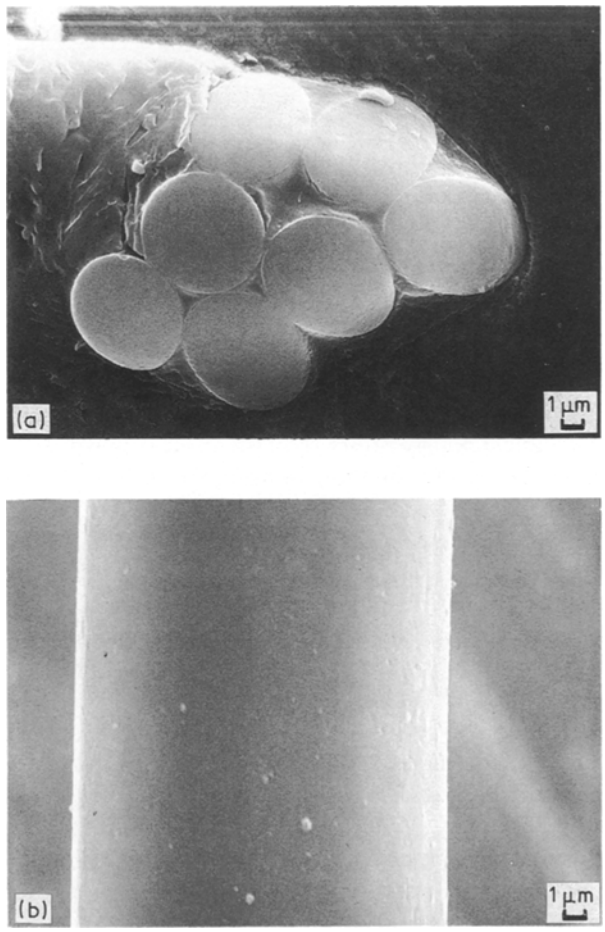

Figure 15 Micrographs of a cross-section (a) and longitudinal view (b) of a microcomposite showing typical geometric irregularities and excellent wetting and uniformity of the epoxy.

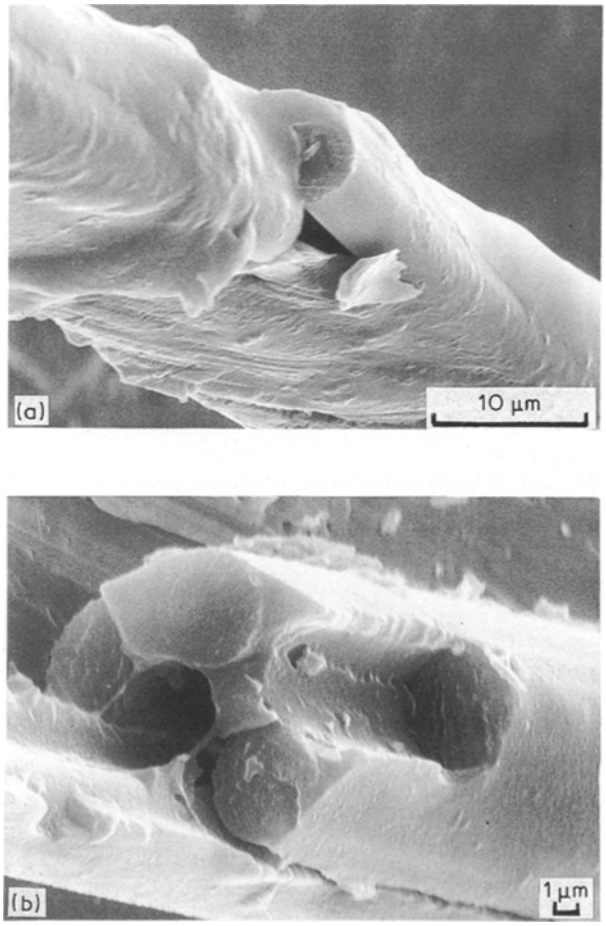

Figure 16 Micrographs of isolated single break (a) and fracture surface (b) in two different specimens.

diameters to the left, and the epoxy appeared to show a mixture of both cracking in between the fibres and debonding from the fibres. In other words, debonding was not "clean" as many torn "chunks" of epoxy could be seen attached to the surface, suggesting excellent adhesion. Around the single fibre break, debonding is apparent but there is also evidence of good epoxy adhesion. Interestingly there appears to be evidence of shear banding and large scale deformation in the epoxy, far beyond the 5 to 7% failure strain of bulk specimen. Other views of this failure surface suggest possible strains of 30 to 50%.

Caution should be exercised in interpreting these micrographs, especially Fig. 16b, since one cannot know the role of wave propagation and resulting buckling and bending after the initial energy release. We saw many cases where failure surfaces were transverse over a longitudinal zone of one or two fibre diameters, but these may not have been the initial fracture zones but rather bending failures due to recoil. Nevertheless, much of the fractographic evidence is consistent with a mixture of epoxy cracking and debonding around fibre breaks as well as large load transfer lengths. Also, time dependent crack growth and debonding is suggested to be a key feature in the creep-rupture process. Unfortunately no fractographic studies were done by Phoenix *et al.* [21] but their fabrication techniques and epoxy viscosities probably led to significantly higher volume fractions of epoxy in their microcomposites.

5.5. Predicted behaviour of large composite structures

As shown in Phoenix *et al.* [1], the value of the power law exponent ρ^* for long times and lower stresses tends to the value $\rho = 2\zeta/(\alpha\theta)$ which lies in the range 27 to 37 depending on our method for arriving at ρ^*. These values are much smaller than values of 80 to 120 which are generally believed to be appropriate on the basis of limited experiments on epoxy-impregnated strands as reported for example by Shaffer [21]. Differences would have to be explained in terms of major differences in matrix creep, the tendency for the fibres to debond from the epoxy, or epoxy volume fraction effects.

5.6. Limiting distribution for bundle strength assuming total debonding

It is interesting to compare the fraction of failed specimens at the end of the experiment with the fraction that would be predicted assuming the seven fibres form a simple bundle with no matrix. For this calculation we use Daniels' classic result [22] for the strength of a loose bundle of fibres including modifications by McCartney and Smith [23] to provide correction terms for small bundles. This result would apply under the assumption that the epoxy matrix eventually debonds completely from the fibre leaving only a loose bundle.

Under this theory a bundle of n fibres has strength which is approximately normally distributed with mean

$$\mu_n = \sigma_l \zeta^{-1/\zeta} e^{-1/\zeta}[1 + 0.966 n^{-2/3} \zeta^{-1/3} e^{2/(3\zeta)}] \quad (41)$$

and standard deviation

$$s_n = \sigma_l \zeta^{-1/\zeta}[e^{-1/\zeta}(1 - e^{-1/\zeta})]^{1/2} \quad (42)$$

From exact numerical calculations, we have found these results to be surprisingly accurate even for a bundle of only seven fibres. For the present fibres of $l = 30$ mm we calculate $\mu_7 = 3966$ MPa and $s_7 = 519$ MPa.

At the 83% stress level (4101 MPa) the fraction of failed bundles is predicted to be 0.603 from this result (using standard normal tables), as compared with the actual fraction 0.90 at the end of the experiment. Accounting for creep-rupture of the individual fibres by adapting the results of Farquhar *et al.* [2], the strength of each fibre at the end of the experiment (4.4×10^6 seconds) is estimated to be about $(4.4 \times 10^6)^{-1/300} = 0.95$ times the starting value, so the mean and standard deviation of the bundle strength would be reduced further to $\mu_7 = 3767$ MPa and $s_7 = 493$ MPa respectively. Thus, at the end of the experiment the fraction of failed bundles is predicted to be 0.75 which is still lower than the fraction 0.90 observed. On the other hand, at the start of the experiment at the 83% stress level, the fraction of

failed microcomposite specimens was observed to be only 0.07 as compared to 0.603 for the simple bundle. Thus we have the interesting situation where the epoxy matrix initially improves the microcomposite strength over that of a simple bundle, but in the end is detrimental to the creep-rupture performance over what one would have achieved with a simple bundle without a matrix.

6. Conclusions

We have generated experimental results on both the strength and the lifetime in creep rupture of carbon–epoxy microcomposites. These composites consisted of seven carbon fibres (Hercules IM6) of almost identical cross-sectional area within an epoxy matrix (Dow DER 332 epoxy with Texaco Jeffamine T403 curing agent) in an approximately hexagonal configuration, and had a gauge length of 30 mm. We also generated extensive statistics on the strength of the single fibres at gauge lengths 10, 30 and 100 mm in order to provide basic information for the model. Special attention was paid to clamping, specimen alignment, shock isolation and accurate lifetime measurement at small times. Thus, some experimental problems encountered in a previous study of Phoenix *et al.* [1] were eliminated. The results were analysed using the theoretical model of these authors, which involves a Weibull distribution for fibre strength and micromechanical stress redistribution around fibre breaks where the matrix creeps or debonds in shear following a power law. The model yields Weibull distribution envelopes for both microcomposite strength and lifetime where the respective shape and scale parameters depend on model parameters such as the Weibull shape parameter for fibre strength, the exponent for matrix creep, and the effective load transfer length and critical cluster size for failed fibres. Depending on the load and time range, the critical cluster size, k, was either two or three. The experimental results were consistent with the theory and compared with results of the earlier study [1] using a different epoxy system (Dow DER 331 epoxy with DEH 26 curing agent). Values for the matrix creep exponent and the effective load transfer length were about double and triple respectively the values from the earlier study, leading to slightly reduced strength, about one-half the variability in lifetime, but almost one-half the value of the exponent for the power law relating microcomposite stress level to lifetime. Effective load transfer lengths were calculated from the model to be sufficiently large at longer times to implicate time-dependent debonding along the fibre–matrix interface or matrix cracking as the dominant mechanism driving the creep rupture process. This view was consistent with the fractographic evidence.

Acknowledgement

This work was supported in part by the Cornell Materials Science Center, an NSF DMR-MRL, and in part under a contract from Martin Marietta Energy Systems, Oak Ridge, Tennessee.

References

1. S. L. PHOENIX, P. SCHWARTZ and H. H. ROBINSON IV, *Composites Sci. Tech.* **32** (1988) 81–120.
2. D. S. FARQUHAR, F. M. MUTRELLE, S. L. PHOENIX and R. L. SMITH, *J. Mater. Sci.* **24** (1989) 2151–2164.
3. A. N. NETRAVALI, R. B. HENSTENBURG, S. L. PHOENIX and P. SCHWARTZ, *Polym. Compos.* **10** (1989) 226–241.
4. A. S. WATSON and R. L. SMITH, *J. Mater. Sci.* **20** (1985) 3260–3270.
5. J. GUTANS and V. TAMUZS, *Mech. Comps. Mater.* **20** (1984) 1107–1109 (in Russian).
6. R. B. HENSTENBURG and S. L. PHOENIX, *Polym. Compos.* **10** (1989) 389–408.
7. R. GULINO and S. L. PHOENIX, *J. Mater. Sci.* (1990) in press.
8. R. L. SMITH, S. L. PHOENIX, M. R. GREENFIELD, R. B. HENSTENBURG and R. E. PITT, *Proc. R. Soc. Lond.* **A388** (1983) 353–391.
9. S. L. PHOENIX and R. L. SMITH, *Int. J. Solid Structures* **19** (1983) 479–496.
10. D. C. LAGOUDAS, C. Y. HUI and S. L. PHOENIX, *ibid.* **25** (1988), 45–66.
11. H. H. ROBINSON IV, H. F. WU, M. AMES and P. SCHWARTZ, *Rev. Sci. Instrum.* **58** (1987) 436–440.
12. H. D. WAGNER, S. L. PHOENIX and P. SCHWARTZ, *J. Compos. Mater.* **18** (1984) 312–338.
13. H. D. WAGNER, *J. Polym. Sci.: Polym. Phys.* **27** (1989) 115–149.
14. A. C. COHEN, *Technometrics* **7** (1965) 579–588.
15. D. D. MASON, "Time Dependence of the Displacement Fields around Fibre Breaks in a Composite with a Power-Law Creeping Matrix", Ph.D. Thesis, Cornell University, Ithaca, N.Y. 14853.
16. R. GULINO, P. SCHWARTZ and S. L. PHOENIX, *J. Mater. Sci.* (1990) in press.
17. R. A. SCHAPERY, *Int. J. Fracture* **11** (1975) 141–159, 369–387, 549–562.
18. R. M. CHRISTENSEN, *J. Rheology* **25** (1981) 517–528.
19. R. M. CHRISTENSEN, and R. E. GLASER, *ASME J. Appl. Mech.* **52** (1985) 1–5.
20. J. M. WHITNEY and L. T. DRZAL, *ASTM STP* 937 (American Society for Testing and Materials, Philadelphia, (1987) 179–196.
21. J. T. SHAFFER in "Materials for Space-The Gathering Momentum, Proceedings of the 18th International SAMPE Technical Conference", edited by J. T. Hoggatt, S. G. Hill, and J. C. Johonson, Seattle WA, 7–9 Oct., 1986.
22. H. E. DANIELS, *Proc. Roy. Soc. London A* **183** (1945) 405–435.
23. L. N. McCARTNEY and R. L. SMITH, *ASME J. Appl. Mech.*, **105** (1983) 601–608.

Received 6 October 1989
and accepted 9 March 1990